Chinese Chemical Letters 35 (2024) 109334

Contents lists available at ScienceDirect

Chinese Chemical Letters

journal homepage: www.elsevier.com/locate/cclet

Insights into the electron transfer mechanisms of peroxydisulfate activation by modified metal-free acetylene black for degradation of sulfisoxazole

Chunxiu Yu[a,b,c], Zelin Wu[a,c], Hongle Shi[b], Lingyun Gu[a,b,c,*], Kexin Chen[b], Chuan-Shu He[a,c], Yang Liu[a,c], Heng Zhang[a,c], Peng Zhou[a,c], Zhaokun Xiong[a,c,*], Bo Lai[a,c]

[a] State Key Laboratory of Hydraulics and Mountain River Engineering, College of Architecture and Environment, Sichuan University, Chengdu 610065, China
[b] Sichuan Academy of Eco-Environmental Sciences, Chengdu 610041, China
[c] Sino-German Centre for Water and Health Research, Sichuan University, Chengdu 610065, China

ARTICLE INFO

Article history:
Received 5 September 2023
Revised 19 November 2023
Accepted 22 November 2023
Available online 25 November 2023

Keywords:
Peroxydisulfate
Sulfisoxazole
Acetylene black
Electrochemical
Electron transfer

ABSTRACT

Herein, a modified metal-free acetylene black (MMF-AB) catalyst was synthesized by a simple solvothermal-calcination method and designed successfully to activate peroxodisulfate (PDS) for the degradation of sulfisoxazole (SIZ). Due to the doping of N, S and O metal-free elements, the modified catalyst showed excellent catalytic performance with 100% SIZ removal within 30 min. *Pseudo* first-order reaction rate constants (evaluating catalytic efficiencies and activity) of MMF-AB ($k_{obs} = 0.105$ min^{-1}) was 3 times higher than pure-AB ($k_{obs} = 0.029$ min^{-1}). Interestingly, it was demonstrated that the reaction system is based on the transfer of electrons from SIZ to PDS to realize an electron-transfer-based mechanism by the evidence of premixing, electron paramagnetic resonance (EPR) spectroscopy, salt-bridge experiments and electrochemical analyses. The introduction of recyclable filtration device solved the secondary pollution caused by the dispersion of the powdered catalyst in the treated water, which further proved the practicality and superiority of the MMF-AB catalyst.

The frequent detection of antibiotics with resistant, persistent, and hard-to-degrade properties in water calls for the exploration of efficient and durable water treatment technologies, as they pose a formidable potential risk to human health and the ecosystem [1–5]. Sulfonamide antibiotics are prescribed in healthcare, veterinary medicine, industry, livestock farming and aquaculture due to their broad-spectrum bacteriostatic effects. Among them, sulfisoxazole (SIZ) and its intermediate transformation products are used as antibiotic analogs for the treatment of urinary tract infections, with long-term residues in external sewage water. For antibiotics in wastewater, conventional technologies such as biological treatment, adsorption, sedimentation, and coagulation, suffer from limited treatment efficiency, high treatment cost and time consuming [6–8]. Note that the advanced oxidation process (AOPs) through the generation of highly reactive oxygen species (ROS) (*e.g.*, sulfate radicals ($SO_4^{\bullet-}$), hydroxyl radical ($^{\bullet}OH$), superoxide radical ($^{\bullet}O_2^-$), singlet oxygen ($^1O_2$) and so on) has placed a high value to degrade and mineralize contaminants [9,10]. Currently, common oxidants in AOPs include peroxodisulfate (PDS), peroxomonosulfate (PMS), hydrogen peroxide (H_2O_2) and ozone (O_3), and peracetic acid (PAA). Compared with PMS and H_2O_2, PDS offers satisfactory advantages in terms of chemical stability and price (PDS \$0.74 per kg *vs.* H_2O_2 \$1.5 per kg *vs.* PMS \$2.2 per kg) [11,12]. Comparatively speaking, it is more favorable to transport, store and handle PDS than H_2O_2, O_3, PAA [13]. On the strength of the two characteristics, PDS-based AOPs stand out in water treatment.

PDS-based AOPs have gained a broad scope of interest in the mineralization of organic pollutants by their outstanding oxidation capacity, wide-ranging adaptability, and great economic and environmental benefits [14–16]. Currently, the methods of activating PDS can be roughly divided into physical (ultraviolet light, alkali, heat, ultrasound) [17–19], homogeneous (transition metal ions) [20], and heterogeneous methods. The heterogeneous activation method (carbon materials, metal oxides (CuO, Fe_2O_3, MnO_2, Co_3O_4), and minerals) is of great interest due to its high activation performance, reduced metal leaching and the absence of additional energy input [21–24].

In particular, it is well documented that carbon-based materials have a good activation effect on the PDS. The secondary contamination associated with metal leaching is eliminated when carbon-based materials are used as catalysts [25–31]. Acetylene black (AB),

* Corresponding authors.
E-mail addresses: glyn0301@126.com (L. Gu), scuxzk@scu.edu.cn (Z. Xiong).

https://doi.org/10.1016/j.cclet.2023.109334
1001-8417/

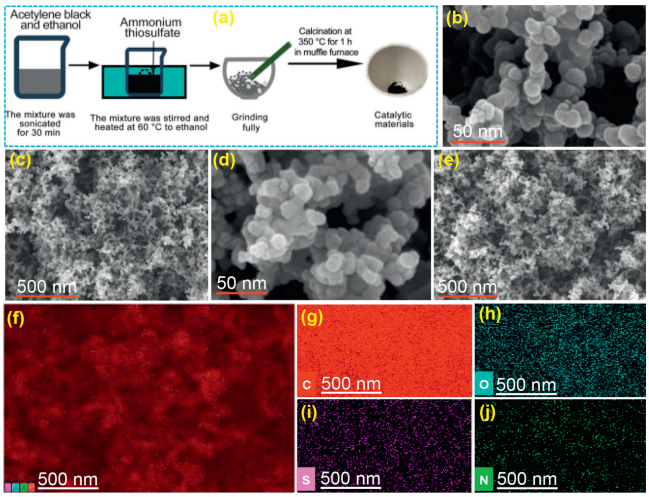

Fig. 1. (a) Schematic diagram of the preparation process of MMF-AB. (b, c) SEM image of MMF-AB with 50 nm and 500 nm, and (d, e) used MMF-AB with 50 nm and 500 nm. EDS element mapping images of MMF-AB (500 nm) (f), C (g), O (h), S (i), N (j).

as a typical carbon material, has the virtue of good electrical conductivity, low price and large specific surface area, and is widely applied as capacitors and electrode materials [32,33]. There have been documents showing that acetylene black has catalytic properties. For example, Si *et al.* found that heavily nitrogen-doped acetylene black can be used as a high-performance catalyst for oxygen reduction reactions [32]. TiO_2 doped with AB was employed with PDS for the degradation of tetracycline hydrochloride (TH) [34]. AB/PDS system can effectively degrade sulfamethoxazole (SMX) [35]. However, there are few studies on modifying or supporting AB to potentiate oxidant activation and thus improve pollutant degradation.

Consequently, in this work, a modified metal-free acetylene black (MMF-AB) catalyst was synthesized by a simple solvothermal-calcination method. We developed an MMF-AB/PDS system using MMF-AB as a PDS activator. The activation performance of MMF-AB was evaluated by taking SIZ as the target model pollutant. Research works mainly include: (1) The physicochemical and photocatalytic properties of MMF-AB were characterized by X-ray diffraction (XRD), scanning electron microscopy (SEM), transmission electron microscope (TEM) and X-ray photoelectron spectroscopy (XPS), Brunner-Emmet-Teller (BET); (2) Optimizing operating parameters such as catalyst dosage, PDS amount, initial pH, temperature; (3) The application of the system in different actual water treatment; (4) The mechanism of MMF-AB/PDS system and degradation pathways of SIZ were investigated. More importantly, to facilitate the recovery and reuse of the catalyst in slow-flowing water, MMF-AB catalytic membrane was prepared with highly efficient degradation.

MMF-AB was synthesized by a facile solvothermal-calcination method (Fig. 1a and Text S1 in Supporting information). As depicted in Figs. 1b and c, the SEM images indicate that the catalyst exhibits a microscopically cross-linked coral-like finely dispersed appearance. It could be clearly seen that the MMF-AB monomer presents a spherical structure with the sphere presenting fine flock particles (Fig. 1b). The monomer catalysts show varying degrees of regularity, culminating in a coral-like structure. The non-smooth spherical surface and multi-channel coral-like structure of the catalyst not only provided a good specific surface area, but also a large number of active sites for the attachment of oxidants. And used MMF-AB had no obvious morphological changes (Figs. 1d and e). The proportion of carbon (C), nitrogen (N), oxygen (O), sulfur (S) elements is analyzed under the 500 nm electron microscope picture for MMF-AB (Figs. 1f-j and Fig. S2 in Supporting information). Relevant EDS element mapping images of MMF-AB revealed that the C, N, O and S elements were uniformly attached to the catalyst surface. Thereinto, a small amount of O and S are also detected, N was the least. This indicated that N, O and S elements have been successfully injected into MMF-AB, which laid the foundation for strengthening the catalytic performance of the catalyst.

Figs. 2a and b display the XRD patterns and FTIR of relative catalysts to verify the crystalline structure. It could be appreciated that there is no distinct difference for pure-AB, MMF-AB, and used MMF-AB. The diffraction peaks at $2\theta = 25°$ and 43.5° correspond to the (002) and (100) plane of the graphite carbon structure to possess specific graphite properties [32,35-37]. It may indicate the low crystallinity and graphitization due to the peak width of the MMF-AB and used MMF-AB at $2\theta = 25°$ were larger compared with pure-AB [38]. To clear the containing functional groups, the FTIR of AB, pure-AB, MMF-AB and different ratios of AB:AT were well supported, which have been shown in Fig. 2b. The absorption peaks at 1065, 1035–1260, 1405, and 2800–3000 cm^{-1} of the modified materials after high-temperature calcination are all enhanced compared with AB. The 1065 cm^{-1}, 1035–1260 cm^{-1}, and 1405 cm^{-1} distinct band is attributed to the stretching vibration peak of -COC-, -C-O and -COO- group [39–41]. The surface area and pore size of pure-AB and MMF-AB were measured by BET measurements (Fig. 2c and Fig. S4 in Supporting information). There was no difference in the surface area between MMF-AB (52.59 m^2/g) and pure-AB (54.93 m^2/g) (Table S2 in Supporting information). In addition, V-type isotherm that the desorption isotherm exceeds the adsorption isotherm and has a hysteresis loop. This indicates that the adsorbate has undergone capillary condensation and has a mesoporous structure [42]. To comparably investigate the electrochemical performance of MMF-AB, pure-AB, and AB, the Tafel curve and electrochemical impedance spectroscopy (EIS) of the catalysts were determined. As highlighted in Fig. 2d, the slope of MMF-AB is the highest in the low-frequency region, which implies that it has the smallest internal charge-transfer resistance, due to the doped N, S, and O elements slowing down the interfacial charge-transfer kinetics. Tafel plots (Fig. 2e) gave free corrosion potentials of −0.448, −0.373, and −0.384 V for MMF-AB, pure-AB, and AB, respectively, revealing that MMF-AB has a higher electron transfer rate and a better catalytic activity.

The chemical composition and elemental content of pure-AB, MMF-AB, and used MMF-AB were visualized by XPS (calibrated at 284.6 eV C 1s). As displayed in Fig. 2f, the measured XPS full spectra plot that the pure-AB only shows C 1s and O 1s, while the MMF-AB and the used MMF-AB gained the peaks intensity of S 2p and N 1s. This implied that the AT-modified AB was successfully doped with N/S elements. Specifically, pure-AB, MMF-AB and used MMF-AB could be decomposed into 531.5 eV, 532.7 eV, and 533.8 eV, corresponding to C=O, C–O, and O–H respectively (Fig. 2g) [43–53]. Elevated oxygen content of materials calcined at high temperatures. Noteworthy, the C 1s spectra can be split into peaks for the carbon-containing functional groups C–H (283.8 eV), C–O (284.8 eV), O=C–C (286.6 eV), C–N (285.7 eV, present in MMF-AB and used MMF-AB) (Fig. S5 in Supporting information) [54–57]. Fig. 2h illustrated the partitioned spectra of N 1s, which could be segmented into N–C, pyridinic N, and graphitic N, separately for MMF-AB and used MMF-AB [58–63]. Graphite N content decreased mainly due to the possible depletion of graphite N as the main active site after the reaction. The post-reaction pyridine N content was reduced due to N adherence in the contaminants. The two peaks located at 168.7 and 169.9 eV can be assigned to S(VI) in sulfates (Fig. 2i), which is formed from the intermediate of ammonium thiosulfate during solvothermal-calcination treatment [64,65]. In summary, N, S, and O elements were successfully doped in AB.

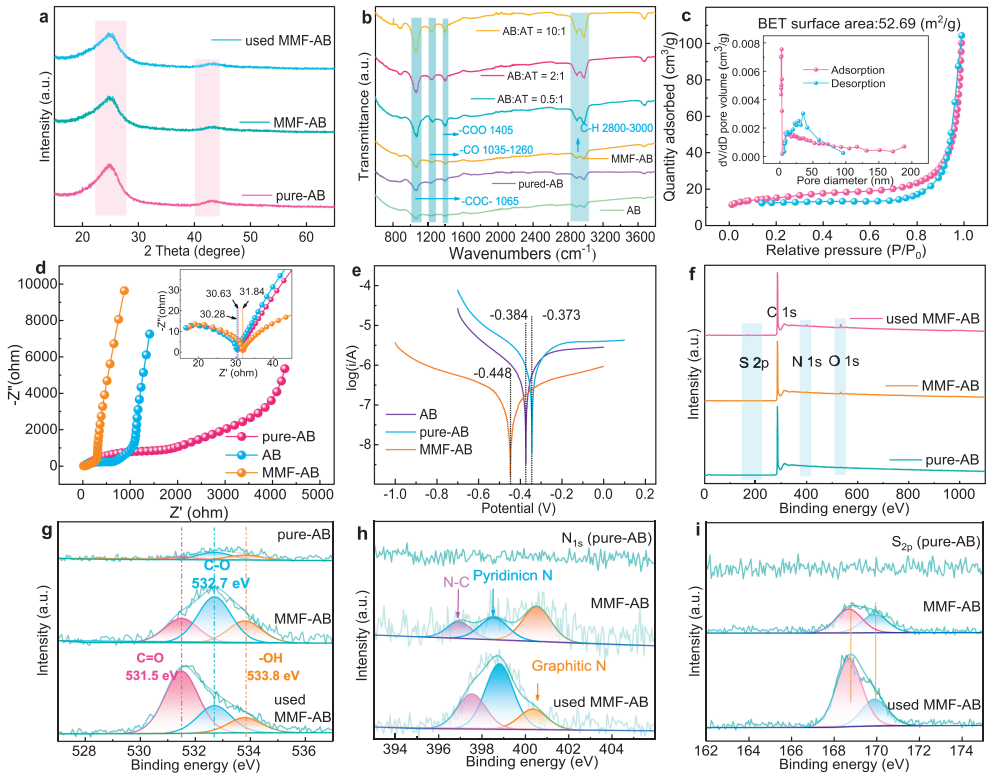

Fig. 2. (a) The XRD patterns. (b) FTIR diagram with different mass ratios of AB and AT. (c) N_2 adsorption-desorption isotherm curves of MMF-AB. (d) electrochemical impedance spectroscopy (EIS) and (e) Tafel polarization curve of pure-AB, AB, and MMF-AB. XPS spectra of (f) full-range scan of the samples, (g) O 1s, (h) N 1s and (i) S 2p core level for MMF-AB, pure-AB and used MMF-AB.

Empirically, five sets of control experiments (pure-AB adsorption, MMF-AB adsorption, AT, MMF-AB, and pure-AB) were undertaken to elicit the catalytic performance of MMF-AB. Figs. 3a and b displayed that the SIZ removal rate by sole modifying agent was only 6.03%. Meanwhile, the adsorption capacity of alone pure-AB (0.45%) and MMF-AB (1.04%) were negligible. With the addition of PDS, the MMF-AB/PDS system removed 95.7% of SIZ compared to 59.36% with pure-AB. *Pseudo* first-order reaction rate constants (evaluating catalytic efficiencies and activity) of MMF-AB ($k_{obs} = 0.105$ min^{-1}) was 3 times higher than pure-AB ($k_{obs} = 0.029$ min^{-1}). The PDS consumption rate was evaluated according to the iodometric method (Text S8 in Supporting information) [66]. In the MMF-AB/PDS and pure-AB/PDS systems, the PDS consumption rate gradually increased during the 30 min treatment. Notably, the MMF-AB/PDS system consumed more PDS (39.68% PDS consumption rate for pure-AB and 62.26% PDS consumption rate for MMF-AB) (Fig. 3c). This indicates that the catalytic performance of the modified catalysts was enhanced, and the degradation of SIZ was prominently facilitated with a $1 + 1 > 2$ effect.

To optimize the process parameters, we conducted batch experiments to investigate some key influencing factors (AB:AT, catalyst dosages, PDS concentration, initial pH, and reaction temperature). Firstly, the influence of AT:AB (mass ratio) on the catalytic effect is shown in Fig. 3d and Fig. S6a (Supporting information) at the catalyst amount of 50 mg/L, the PDS concentration of 0.1 mmol/L and SIZ (5 mg/L). With the increasing amount of AT (AB:AT = 1:0, 1:0.1, 1:0.5, 1:1, 1:2, 1:10), the degradation effect of SIZ gradually elevated (59.3%, 72.70%, 89.7%, 95.8%, 91.7%, 92.1%) and then gradually stabilized. The corresponding reaction rate also increased from $k_{obs} = 0.029$ min^{-1} to $k_{obs} = 0.105$ min^{-1}. Subsequently, excellent removal was achieved that the degradation rate increased from 29.80% to 100% and the reaction rate raised from 0.011 min^{-1} to 0.244 min^{-1} with MMF-AB dosage in the circle of 10–100 mg/L (Fig. 3e and Fig. S6b in Supporting information). By increasing the catalyst dosage to 150 mg/L, SIZ could be completely removed within 30 min. Generally, an increasing number of catalysts means more adsorption and activation sites for PDS [67]. When the amount of PDS increased from 0.02 mmol/L to 0.05 mmol/L, 0.07 mmol/L, 0.1 mmol/L, k_{obs} raised from 0.137 min^{-1} to 0.198 min^{-1}, 0.24 min^{-1}, 0.244 min^{-1} (Fig. 3f and Fig. S6c in Supporting information). SIZ was completely degraded within 30 min when more than or equal to 0.05 mmol/L PDS was respectively added. Additionally, the k_{obs} of SIZ removal no longer increased ($k_{obs} = 0.18$ min^{-1} (0.2 mmol/L), $k_{obs} = 0.148$ min^{-1} (0.3 mmol/L)) with further increasing PDS concentration. This may be caused by redundant PDS taking up the active site [68]. Therefore, taking into account the economic and approximate degradation efficiency, the key parameter of the 1:1 ratio of AB:AT, 100 mg/L of MMF-AB, and PDS concentration (0.1 mmol/L) were selected as the practical condition.

On this basis, the effect of the initial concentration of SIZ on the removal effect was investigated (Fig. 3g and Fig. S6d in Supporting information). The degradation effect and reaction rate gradually decreased with increasing from 1 mg/L SIZ concentration to 20 mg/L (Text S9 in Supporting information). Fig. 3h demonstrated that the removal of SIZ held in the range of 95% to 100% at initial pH values from 3 to 9 (Text S10 in Supporting information). In accordance with the graph of Fig. 3i and Fig. S6e (Supporting information), the degradation effect of the system on SIZ reached more than 93% at 10–40 °C, and partially elevated temperature was favorable for the reaction (Text S11 in Supporting information).

Many coexisting anions and humic acids (HA) existing in actual water bodies make a perceptible difference to the target pollutants due to competing with the target pollutants for ROS and hinder the practical application from laboratories to plants [69,70]. Hence, it is necessary to study their impact on the MMF-AB/PDS system.

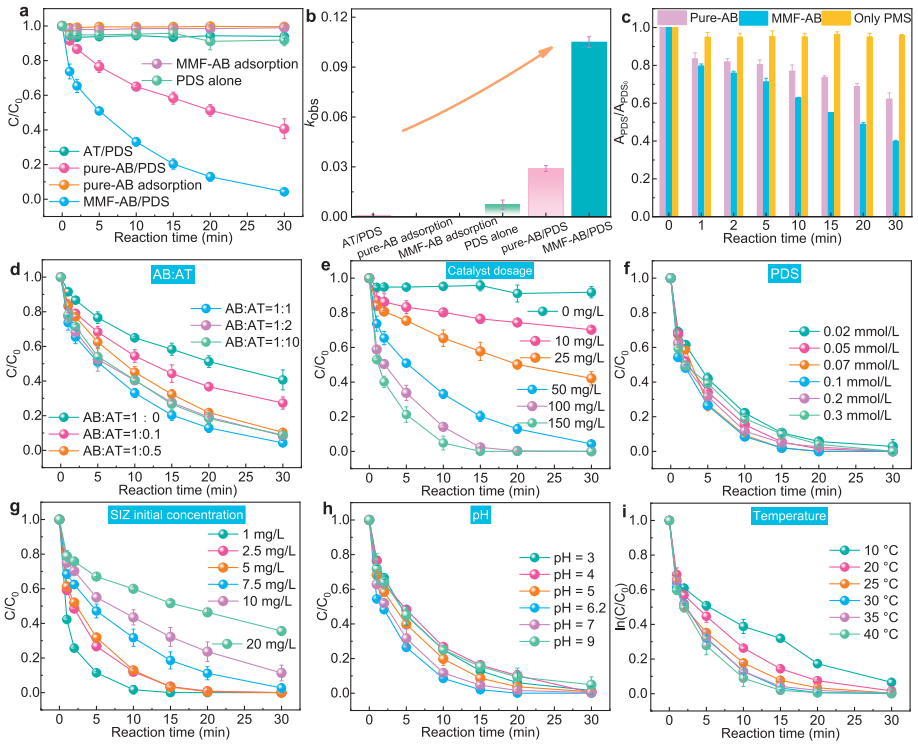

Fig. 3. (a, b) SIZ removal efficiencies and corresponding k_{obs} by different systems, (c) PDS residual rate. The influence of distinct experimental parameters of (d) different AB:AT, (e) catalyst dosage, (f) PDS concentration, (g) SIZ initial concentration, (h) different initial pH, (i) reaction temperature. Experiment conditions: reaction time = 30 min, T = 30 °C, rotating speed of stirring = 300 rpm.

In this work, we evaluated the following anions, such as phosphate ($H_2PO_4^-$), nitrate (NO_3^-), chloride (Cl^-) (in the range of 1–10 mmol/L), and HA (1–10 mg/L) on the erasure of SIZ. In particular, the inhibitory effect of representative inorganic anions and HA on the system exhibited as follows: $H_2PO_4^- < Cl^- < NO_3^- <$ HA (Fig. 4a and Text S12 in Supporting information). Overall, the additional addition of inorganic anions and HA created a competitive relationship with the pollutant SIZ, due to the fact that the inorganic anions react with the non-radicals, thus decreasing the chances of the non-radicals degrading the SIZ. In addition, we explored the effectiveness of the system in removing different pollutants. Fig. 4b demonstrated the following removal rates for different pollutants under the same conditions: SIZ (100%), BPA (92.34%), LVF (91.67%) and NOR (99.84%). This outcome revealed that the system was effective in removing common pollutants. To evaluate the biological toxicity during the degradation process, the water quality biological toxicity during the degradation process was tested by Luminescent bacteria with *Vibrio fischeri* [71,72]. Toxicity inhibition rate (IR) in the range of <30%, 30%–80%, >80% indicates that the solution is of respectively low toxicity, toxic, and highly toxic. In this reaction system, the initial toxicity inhibition rate was 17.26%, the toxicity inhibition rate increased to 32.10% after 10 min of reaction, and the toxicity inhibition rate decreased to 6.41% after the end of the reaction (30 min) (Fig. 4c). It shows that some highly toxic intermediates are easily attacked and degraded into less toxic products.

More importantly, the intermediate product of SIZ in the MMF-AB/PDS system was determined by UPLC-QTOF-MS/MS. Six possible intermediates were determined by the accurate masses of the primary products and their main fragments (Figs. S8-S14 in Supporting information). As depicted in Fig. 4d, with the foundation of the experimental and antecedent research results, possible degradation pathways of SIZ were proposed. Firstly, as shown in path I, **P1** and **P2** could be produced by the breaking of the C–N bond in the SIZ. And product **P3** might be detected due to azo combining reaction [73,74]. Furthermore, pathway II may be analyzed due to the formation of product **P4** and **P5** as the splitting of S-N bond [75,76]. In addition, **P6** that lacks a methyl group from SIZ was also detected [74,77]. Normally, these intermediates are mineralized into low-molecular substances such as H_2O, CO_2, and other mineral compounds under the MMF-AB/PDS system. In order to further study the variability of the toxic effects of SIZ and 6 intermediate products, the quantitative structure-activity relationship (QSAR) method was applied to investigate the relative strength of the mutagenicity, acute toxicity (LD_{50}), bioaccumulation factor and developmental toxicity for TP_x-SIZ by using Toxicity Estimation Software Tool (T.E.S.T., US, EPA) (Figs. 4e-h) [10,78]. Overall, the toxicity of the intermediate products that may be derived from the removal process has been reduced relative to the SIZ, but some intermediates are still relatively toxic. Specifically, the SIZ and 5 TPs showed negative mutagenicity after MMF-AB/PDS oxidation (Fig. 4e). And the oral rat dose of the 5 TPs is lower than SIZ, indicating increased toxicity in oral rats (Fig. 4f). Additionally, 6 TPs had lower bioaccumulation factor than SIZ (Fig. 4g). The toxicity of 3 intermediates is lower than that of SIZ, and the toxicity of 3 intermediates is higher for developmental toxicity (Fig. 4h). This explains why acute toxicity first increases at 10 min of reaction and then decreases to non-toxicity.

In depth, specific quenchers are utilized to capture potential ROS in the reaction system and EPR is in place to further confirm the generated ROS. Among them, TBA and MeOH served as inhibitors of $^{\bullet}OH$ and $SO_4^{\bullet-}$ [79], NaN_3 and L-histidine are used as indicators of singlet oxygen ($^1O_2$) [80], and *p*-BQ regarded as a scavenger of superoxide radicals ($^{\bullet}O_2^-$) [81,82]. As shown in Fig. 5a, the degradation rates were 86.68% and 98.71% respectively when 1 mol/L MeOH and TBA were added to the MMF-AB/PDS system. It was concluded that the two quenchers slightly inhibited the degradation of SIZ.

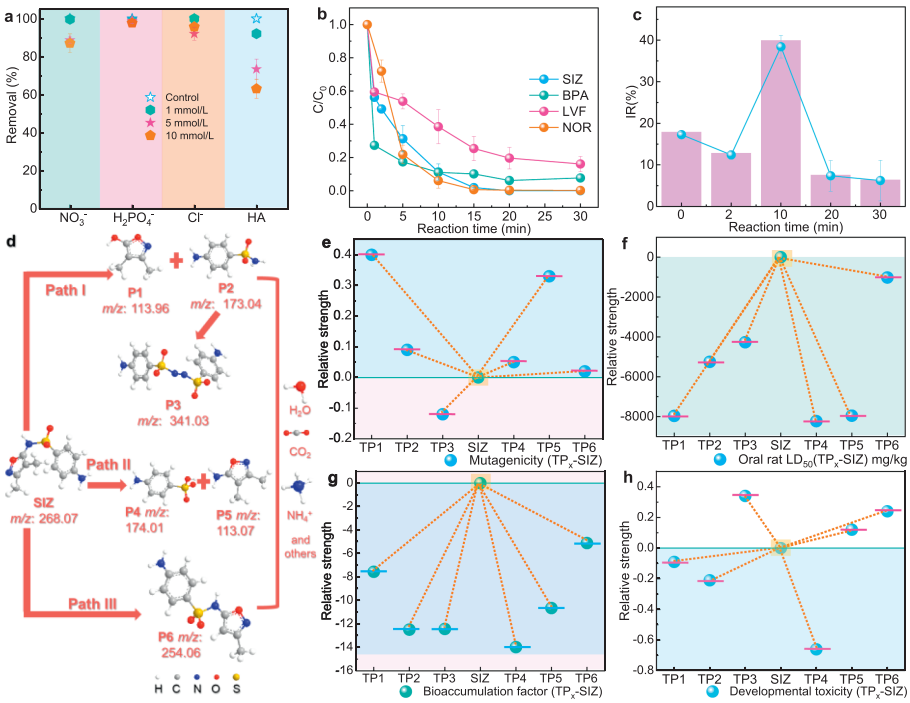

Fig. 4. (a) Effects of co-existing anion and HA on SIZ degradation in MMF-AB/PDS system. (b) Removal effect of different pollutants in the system. (c) Biological toxicity test of MMF-AB/PDS system. (d) Possible transformation pathways of SIZ in MMF-AB/PDS system. Relative strength of (e) mutagenicity, (f) acute toxicity, (g) bioaccumulation factor, and (h) developmental toxicity for TP_x-SIZ. (Experimental conditions: $[SIZ]_0$ = 5 mg/L, $[catalyst]_0$ = 100 mg/L, $[PDS]_0$ = 0.1 mmol/L, reaction time = 30 min, T = 30 °C, rotating speed of stirring = 300 rpm).

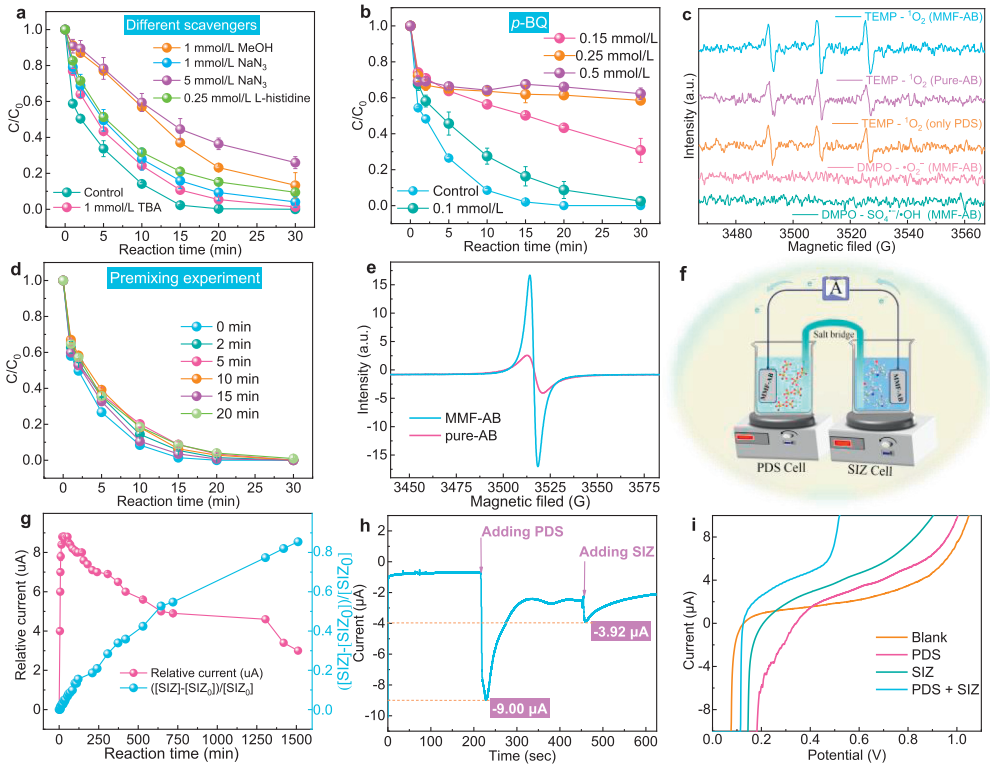

Fig. 5. (a) The effects of different scavengers (TBA, MeOH, L-histidine, NaN_3) on SIZ degradation efficiency in MMF-AB/PDS system. (b) The inhibition efficiency of SIZ degradation by different *p*-BQ concentrations. Experimental conditions: $[SIZ]_0$ = 5 mg/L, $[catalyst]_0$ = 100 mg/L, $[PDS]_0$ = 0.1 mmol/L, reaction time = 30 min, T = 30 °C, rotating speed of stirring = 300 rpm. (c) EPR spectra of $^1O_2$, $^{\bullet}O_2^-$, $^{\bullet}OH$, $SO_4^{\bullet-}$ in MMF-AB/PDS system. (d) Influence of different pre-mixing time on the degradation effect of SIZ. (e) EPR spectra of MMF-AB (g = 2.006). (f) The galvanic oxidation process reaction device setup. (g) Current change from the PDS cell to the SIZ cell and SIZ oxidation in the galvanic oxidation process. (h) Chronoamperometry curve (I-t) measurement upon the addition of respectively PDS and SIZ using MMF-AB as the working electrode. (i) LSV curves. (Conditions: $[Na_2SO_4]_0$ = 0.5 mol/L, $[PDS]_0$ = 0.1 mmol/L, $[SIZ]_0$ = 5 mg/L).

Moreover, when 1 mol/L MeOH and TBA were respectively added to the 0.1 mmol/L PDS solution, only 1.64% of PDS was used up for MeOH and 1.77% of PDS was consumed for TBA (Fig. S15a in Supporting information). Furthermore, as depicted in Fig. 5b, no significant $^{\bullet}OH$ and $SO_4^{\bullet-}$ signals were captured by EPR experiments using DMPO as a spin trapping agent. Therefore, according to quenching experiments and EPR experiments, it is found that $^{\bullet}OH$ and $SO_4^{\bullet-}$ are not the main radicals involved in the degradation of SIZ in the MMF-AB/PDS system. Secondly, the role of $^1O_2$ in this system was studied. As revealed in Fig. 5a, the degradation efficiency of SIZ was attenuated by 94.96% and 74.05% when 1 mmol/L and 5 mmol/L NaN_3 were added, respectively. According to Fig. S15b (Supporting information), 5 mmol/L NaN_3 could consume 35.97% of 0.1 mmol/L PDS. Therefore, the possibility cannot be ruled out that the addition of NaN_3 consumed PDS in the system, resulting in a decrease in the degradation rate. Besides, many literatures have reported that L-histidine could quench $^1O_2$. When 0.25 mmol/L L-histidine was introduced, the removal rate dropped from 100% to 90%. EPR experiments were completed to capture $^1O_2$ by utilizing TEMP as the spin-trapping agent in MMF-AB/PDS, pure-AB/PDS, and PDS systems. The EPR test showed that PDS alone, pure-AB/PDS, and MMF-AB/PDS had characteristic peaks of $^1O_2$, and the characteristic peak of the $^1O_2$ produced by MMF-AB/PDS is slightly stronger than two (Fig. 5c). In summary, in this reaction system, $^1O_2$ might be produced to participate in the degradation of SIZ. The $^1O_2$ mainly came from the self-decomposition of PDS [83], and the $^1O_2$ generated by the material attacking PDS was extremely small.

Subsequently, we utilized the quencher *p*-BQ and EPR to verify $^{\bullet}O_2^-$ (Fig. 5b). With the addition of 0.1 mmol/L, 0.15 mmol/L, 0.25 mmol/L, 0.5 mmol/L *p*-BQ to the experimental system, the degradation effect of SIZ decreased from 100% to 97.54%, 69.26%, 41.49%, and 37.75%, respectively. This experimental phenomenon shows that the system shows an inhibitory effect on the degradation of SIZ after adding the quencher *p*-BQ. In addition, according to Fig. S15c (Supporting information), 1 mmol/L of *p*-BQ consumed 41.23% of PDS (0.1 mmol/L) after 30 min of reaction. In accordance with EPR tests, no distinctly characteristic peaks of $^{\bullet}O_2^-$ were detected (Fig. 5c). In summary, the quenching phenomenon exhibited by the *p*-BQ as a quenching agent may be mainly due to the consumption of PDS.

Aforementioned results indicate that ROS might not play a major role in this system. To determine whether this system was an electron transfer system, the pre-mixing experiment, solid EPR, salt bridge experiment, and electrochemical analysis were adopted to prove it. Firstly, the change of degradation rate and the PDS remaining rate was explored through pre-mixing experiments. Specifically, the removal of SIZ was detected by reacting the catalyst with PDS for different intervals before adding pollutants. It was found that the degradation rates of SIZ were 100%, 100%, 100%, 99.10%, 97.36%, and 99.11%, respectively corresponding to 0, 2, 5, 10, 15, and 20 min of pre-mixing (Fig. 5d). In addition, the remaining rate of PDS corresponding to different pre-mixing times was measured, and it is discovered that only 15.10% of 0.1 mmol/L PDS was consumed after pre-mixing for 20 min (Fig. S15d in Supporting information). The bottom line might indicate that most of the PDS are not attacked and consumed by the catalyst, and ROS not be directly and fractionally amount generated through direct contact between the two. The materials were investigated for the formation of vacancies based on solid-state EPR tests. The catalyst showed a signal at $g = 2.006$, while the EPR response was stronger for the modified catalyst. It shows that the modified material has more vacancies, which in turn forms more unpaired electrons [84,85]. This phenomenon might provide an effective pathway for electron transfer, thereby promoting catalytic activity (Fig. 5e).

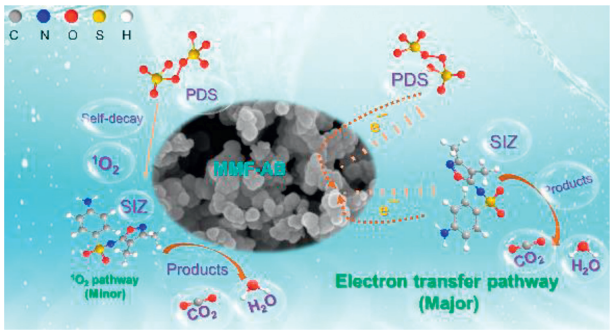

Fig. 6. Non-free radical degradation mechanism diagram in MMF-AB/PDS system.

Relatively, to slightly further testify the electron transfer mechanism in the MMF-AB/PDS system, the salt bridge experiment was applied to monitor the changes of current and SIZ concentration (Fig. 5f) [86]. In this experiment, SIZ could only be degraded through electron transfer with the SIZ and PDS are severally placed in two half-cell beakers. When the MMF-AB was not coated on the graphite electrode and other test conditions were the same, no obvious degradation of SIZ and continuous change of current were detected during the reaction. Since the MMF-AB is uniformly coated on the graphite electrode in the two half-cells after adding PDS, the maximum current value (9 μA) is detected 20 min later. As time goes by, the current drops extremely slowly, and the system still maintains a current of 2 μA after 30 h. At the same time, the degradation effect of this system on SIZ slowly increased and reached 84.66% after 30 h (Fig. 5g). Based on the above experimental phenomena, it is shown that SIZ could be oxidized through the direct electron transfer pathway.

Electrochemical measurements further prove the non-radical pathway of electron transfer in MMF-AB system. Subsequently, the chronoamperometry was developed to survey the electron transfer between the catalyst, PDS and SIZ as shown in Fig. 5h. Firstly, after adding PDS to the Na_2SO_4 electrolyte, the current instantly moved from −1.00 μA to −9 μA. The phenomenon primarily stems from the truth that an electron transfer complex (PDS interacts with MMF-AB) was formed due to electrons translating instantaneously from MMF-AB to PDS [87]. Then, the current instantly moved from −3.00 μA to −3.92 μA. This might form an electron transfer complex between SIZ and MMF-AB after adding SIZ [88]. Furthermore, the linear sweep voltammetry (LSV) test was further used to illustrate the reaction mechanism in the system. As shown in Fig. 5i, when PDS, SIZ, SIZ + PDS severally are added to the Na_2SO_4 solution in sequence, the current transmission effect was SIZ/PDS/MMF-AB > SIZ/MMF-AB > PDS/MMF-AB > MMF-AB. Adding PDS and SIZ to the electrolyte concurrently, the current change of the SIZ/PDS/MMF-AB was significantly higher than the above three. This result directly proved that the interaction between PDS and MMF-AB formed a metastable reaction complex, and electrons are relocated from SIZ to surface-limited no radical species [89,90]. In summary, the test results based on chronoamperometry and LSV directly demonstrated that the reaction system was principally dominated by the electron transfer mechanism.

The foregoing analysis concluded that a non-radical dominated degradation mechanism of the MMF-AB/PDS system was summarized in Fig. 6. In the first place, the $^1O_2$ that mainly came from self-decay with PDS and marginally produced by attacking PDS through the catalyst in ROS participates in the reaction. More importantly, electron transfer mechanism is identified as a matter of priority in the MMF-AB/PDS system. The specific details are as follows [88]:

$$S_2O_8^{2-} + \text{MMF-AB} \rightarrow [\text{MMF-AB—PDS}]^* \quad (1)$$

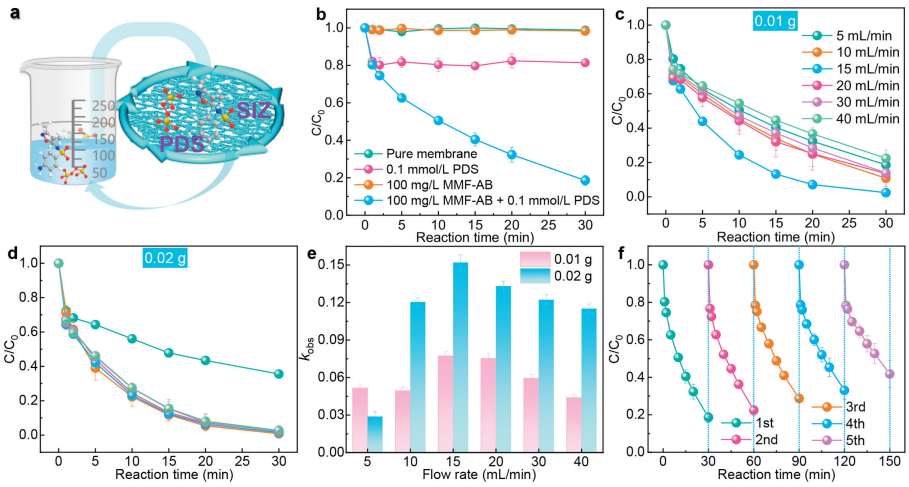

Fig. 7. (a) Schematic diagram of the degradation SIZ for recyclable filtration devices. (b) The degradation effect of SIZ in the recyclable filtration device. (c-e) SIZ removal and k_{obs} value under different flow rates with 0.01 g catalyst and 0.02 g catalyst, respectively. (f) Circulation experiment in recyclable filtration device. Reaction conditions for (a) and (d): AB:AT = 1:1, $[PDS]_0$ = 0.1 mmol/L, $[SIZ]_0$ = 5 mg/L, T = 30 °C, $Catalyst_0$ = 0.01 g, L = 100 mL, flow rate = 5 mL/min.

$$SIZ + [MMF\text{-}AB—PDS]^* \rightarrow [SIZ + [MMF\text{-}AB—PDS]^*]^* \quad (2)$$

$$[SIZ + [MMF\text{-}AB—PDS]^*]^* \rightarrow Products + SO_4^{2-} + [MMF\text{-}AB] \quad (3)$$

where [MMF-AB—PDS]* is complex between PDS and MMF-AB, and among SIZ and [MMF-AB—PDS]* formed electron-transfer complex [SIZ + [MMF-AB—PDS]*]*, reacted MMF-AB was denoted as [MMF-AB]. SIZ and [MMF-AB—PDS]* formed an electron transfer complex to achieve SIZ degradation. Therefore, rather than the general mechanism of ROS, this MMF-AB/PDS system has undergone a non-radical pathway dominated by electron transfer.

Given that, it is definitely confirmed that MMF-AB/PDS has excellent catalytic degradation ability for SIZ. However, the stagnation of the reacted MMF-AB powder in water is a source of secondary contamination and increases the cost of recycling. Therefore, a catalytic MMF-AB membrane and a circulating filter device were designed and constructed to activate PDS for degradation SIZ (Fig. 7a, Text S2 and Text S4 in Supporting information). The analytical results verified that it was extremely difficult to degrade SIZ in the device with pure membrane and catalyst alone. 18.60% of SIZ was removed in 30 min with the only addition of PDS (Fig. 7b). Surprisingly, 81.43% of SIZ was withdrawn with the addition of PDS. This indicated that the MMF-AB/PDS filtration system has had a favorable performance in this installation. This is mainly due to the shortened contact spacing between the ROS and the contaminants generated by the repeated stacking of the MMF-AB catalyst on the membrane in full intimate contact with the oxidant, resulting in good degradation of SIZ.

In addition, the influence of the water flow rate was calibrated on the degradation effect of SIZ. It was determined that the degradation effect for SIZ displayed a trend of first increment to the maximum and then slightly decreasing with the increase of water flow rate. By controlling the water flow rate, the catalyst dosage of 0.01 g and 0.02 g showed the same pattern (Figs. 7c-e). This is mainly because the number of cycles increased at the same time as the flow rate increased, which led to an increase in the chance of pollutants contacting the catalyst. However, as the flow rate improves, the unit hydraulic retention time decreases, and the contact between pollutants and catalysts is greatly shortened. At the same time, in the same cycle experiment, the degradation rate decreased by only 15.02% after 5 cycles, which shows that the device has good stability to the degradation of SIZ (Fig. 7f). The possible reason for the SIZ degradation rate slight decrease after multiple cycles is that multiple shocks of the solution over a long period of time resulted in the collapse of the catalyst causing the pores to become slightly clogged, which led to a decrease in direct contact between the contaminants and PDS and the catalyst.

All in all, MMF-AB was successfully prepared by a simple in-situ evaporation method. Investigation proved that MMF-AB has good activation ability for PDS. Under optimal experimental conditions, the MMF-AB/PDS system achieved 100% removal of SIZ and was highly adaptable to changes in the water environment (*e.g.*, temperature, pH, and common anions). Furthermore, the mechanism of the system has been thoroughly investigated in light of free radical scavenging experiments and EPR. An evidently non-radical mechanism dominated by infinitesimally $^1O_2$ and electron transfer in the MMF-AB/PDS system was validated by pre-mixing experiments, salt bridge experiments, and electrochemical tests. In addition, a rational degradation pathway of SIZ was proposed along with 6 oxidation intermediates. The introduced membrane filtration recycling device not only solved the secondary pollution caused by the powdered catalyst dispersion in the treated water, but also had a good degradation effect on SIZ. In particular, we anticipated that this work would shed new inspirations on the mechanism of persulfate-AOPs reactions and the reconciliation of degradation in practical wastewater treatments.

Declaration of competing interest

The authors declare that they have no known competing financial interests or personal relationships that could have appeared to influence the work reported in this paper.

Acknowledgments

The authors would like to acknowledge the financial support from Sichuan Program of Science and Technology (Nos. 2023NSFSC0344, 2023JDZH0010), the National Natural Science Foundation of China (No. 52200105), the National Key Research and Development Program of China (No. 2021YFA1202500). The authors also would like to thank the Analytical & Testing Center of Sichuan University for EPR detection.

Supplementary materials

Supplementary material associated with this article can be found, in the online version, at doi:10.1016/j.cclet.2023.109334.

References

[1] J. Liu, O. Gefen, I. Ronin, et al., Science 367 (2020) 200–204.
[2] Y. Yang, Y.S. Ok, K.H. Kim, et al., Sci. Total Environ. 596 (597) (2017) 303–320.
[3] Y. Song, S. Gao, J. Tian, et al., J. Environ. Chem. Eng. 8 (2020) 104390.
[4] D.I. Andersson, D. Hughes, Nat. Rev. Microbiol. 12 (2014) 465–478.
[5] Q.Q. Zhang, G.G. Ying, C.G. Pan, et al., Environ. Sci. Technol. 49 (2015) 6772–6782.
[6] D. Cheng, H.H. Ngo, W. Guo, et al., Bioresour. Technol. 319 (2021) 124160.
[7] F. Yin, S. Lin, X. Zhou, et al., Sci. Total Environ. 759 (2021) 143520.
[8] K.J. Choi, S.G. Kim, S.H. Kim, J. Hazard. Mater. 151 (2008) 38–43.
[9] F. Liu, H. Zhou, Z. Pan, et al., J. Hazard. Mater. 400 (2020) 123322.
[10] L. Lai, H. Ji, H. Zhang, et al., Appl. Catal. B 282 (2021) 119559.
[11] T. Zhang, Y. Chen, Y. Wang, et al., Environ. Sci. Technol. 48 (2014) 5868–5875.
[12] G.P. Anipsitakis, D.D. Dionysiou, Environ. Sci. Technol. 37 (2003) 4790–4797.
[13] X. Duan, H. Sun, J. Kang, et al., ACS Catal. 5 (2015) 4629–4636.
[14] L. Donghao, Z. Shixuan, L. Shengnan, et al., J. Cleaner Prod. 397 (2023) 136468.
[15] V. Hasija, V.H. Nguyen, A. Kumar, et al., J. Hazard. Mater. 413 (2021) 125324.
[16] N. Li, Y. Wang, X. Cheng, et al., Water Res. 222 (2022) 118896.
[17] J. Wang, S. Wang, Chem. Eng. J. 334 (2018) 1502–1517.
[18] M. Nihemaiti, D.B. Miklos, U. Hübner, et al., Water Res. 145 (2018) 487–497.
[19] P. Devi, U. Das, A.K. Dalai, Sci. Total Environ. 571 (2016) 643–657.
[20] H. Liu, T.A. Bruton, F.M. Doyle, D.L. Sedlak, Environ. Sci. Technol. 48 (2014) 10330–10336.
[21] Q. Wang, D. Zhou, K. Lin, X. Chen, Chem. Eng. J. 419 (2021) 129667.
[22] H. Fu, H. Luo, Q. Lin, et al., Chem. Eng. J. 409 (2021) 128201.
[23] Z. Wu, Y. Wang, Z. Xiong, et al., Appl. Catal. B 277 (2020) 119136.
[24] H. Yin, F. Yao, Z. Pi, et al., J. Colloid Interface Sci. 586 (2021) 551–562.
[25] W. Huang, S. Xiao, H. Zhong, et al., Chem. Eng. J. 418 (2021) 129297.
[26] C. Minxian, Z. Yichu, L. Bo, et al., Chem. Eng. J. 455 (2023) 140615.
[27] C. Guan, J. Jiang, Y. Shen, et al., Environ. Sci. Technol. 53 (2019) 9054–9062.
[28] Y. Yang, X. Li, C. Zhou, et al., Water Res. 184 (2020) 116200.
[29] P.-F. Xiao, L. An, D.-D. Wu, New Carbon Materials 35 (2020) 667–683.
[30] G. Liu, T. Zhang, T. Wang, et al., Appl. Catal. B 296 (2021) 120370.
[31] L. Wu, Q. Lin, H. Fu, et al., J. Hazard. Mater. 422 (2022) 126949.
[32] Y. Si, M.G. Park, Z.P. Cano, et al., Carbon 117 (2017) 12–19.
[33] S. Tang, H. Shen, Y. Hao, et al., Biosens. Bioelectron. 104 (2018) 72–78.
[34] T. Zhang, Y. Liu, Y. Rao, et al., Chem. Eng. J. 384 (2020) 123350.
[35] S. Nimai, H. Zhang, Z. Wu, et al., Chin. Chem. Lett. 31 (2020) 2657–2660.
[36] J. Tang, J. Yang, X. Zhou, et al., Microporous Mesoporous Mater. 193 (2014) 54–60.
[37] Q. Wu, Y. Zhu, T. Jiang, M. Li, Int. J. Hydrogen Energy 44 (2019) 23547–23555.
[38] F. Liang, L. Lin, Z. Feng, et al., J. Mater. Chem. A 7 (2019) 8765–8770.
[39] Y. Shen, T. Li, K. Xu, et al., J. Nanopart. Res. 20 (2018) 200.
[40] R.V. Moharir, S. Kumar, J. Clean. Prod. 298 (2021) 126670.
[41] J. Zhao, C. Liu, T. Hou, et al., Bioresour. Technol. 345 (2021) 126545.
[42] L. Lai, H. Zhou, B. Lai, Chem. Eng. J. 349 (2018) 633–645.
[43] H. Ren, F. Qi, A. Labidi, et al., Appl. Catal. B 330 (2023) 122587.
[44] W. Ye, W. Zhang, X. Hu, et al., Sci. Total Environ. 732 (2020) 139245.
[45] Y. Liu, Y. Wang, H. Wang, et al., Appl. Surf. Sci. 492 (2019) 455–463.
[46] V.P. Padmanabhan, R. Kulandaivelu, S.N.T.S. Nellaiappan, Mater. Sci. Eng. C 92 (2018) 685–693.
[47] R. Binions, C.J. Carmalt, I.P. Parkin, et al., Chem. Mater. 16 (2004) 2489–2493.
[48] C.M. Kim, H.S. Jeong, E.H. Kim, Surf. Sci. 459 (2000) L457–L461.
[49] R. Burgess, C. Buono, P.R. Davies, et al., J. Catal. 323 (2015) 10–18.
[50] B. Huang, X. Ren, J. Zhao, et al., Environ. Sci. Technol. 57 (2023) 14071–14081.
[51] X. Wang, Z. Xiong, H. Shi, et al., Appl. Catal. B 329 (2023) 122569.
[52] Y. Hong, H. Zhou, Z. Xiong, et al., Chem. Eng. J. 391 (2020) 123604.
[53] Z. Chen, L. Wang, H. Xu, Q. Wen, Chem. Eng. J. 389 (2020) 124345.
[54] R.J. Levis, L.A. Delouise, E.J. White, N. Winograd, Surf. Sci. 230 (1990) 35–46.
[55] S. Liu, Z.J. Xin, Y.J. Lei, et al., ACS Sustain. Chem. Eng. 5 (2017) 7496–7501.
[56] A.S. Sarac, Microelectron. Eng. 83 (2006) 1534–1537.
[57] G. Beshkov, D.B. Dimitrov, S. Georgiev, et al., Diam. Relat. Mater. 8 (1999) 591–594.
[58] F. Li, H. Zhang, M. Zhang, et al., ACS Sustain. Chem. Eng. 10 (2021) 194–203.
[59] P. Yan, J. Liu, S. Yuan, et al., Appl. Surf. Sci. 445 (2018) 398–403.
[60] S. Yu, D. Yunxuan, Z. Peili, et al., Chin. J. Catal. 43 (2022) 2405–2413.
[61] X. Song, Y. Shi, Z. Wu, et al., Appl. Catal. B 340 (2024) 123240.
[62] Z. Wu, B. Huang, X. Wang, et al., Environ. Sci. Technol. 57 (2023) 14046–14057.
[63] B. Huang, Z. Wu, X. Wang, et al., Environ. Sci. Technol. 57 (2023) 15667–15679.
[64] J.J. Ni, W. Wang, C. Wu, et al., Adv. Mater. 29 (2016) 1605607.
[65] J. Fu, C. Bie, B. Cheng, et al., ACS Sustain. Chem. Eng. 6 (2018) 2767–2779.
[66] H. Zhou, L. Lai, Y. Wan, et al., Chem. Eng. J. 384 (2020) 123264.
[67] L. Tang, Y. Liu, J. Wang, et al., Appl. Catal. B 231 (2018) 1–10.
[68] N. Du, Y. Liu, Q. Li, et al., Chem. Eng. J. 413 (2021) 127545.
[69] M. Li, Q. Wen, Y. Zhang, Z. Chen, Water Res. 221 (2022) 118789.
[70] M. Li, Q. Wen, Z. Chen, et al., Chemosphere 244 (2020) 125449.
[71] L. Lai, P. Zhou, H. Zhou, et al., Appl. Catal. B 297 (2021) 120470.
[72] Z. Chen, M. Li, Q. Wen, Chemosphere 189 (2017) 426–434.
[73] Z. Wang, Z. Wang, W. Li, Y. Lan, C. Chen, Chem. Eng. J. 427 (2022) 130888.
[74] L. Liu, Y. Li, W. Li, et al., Environ. Res. 187 (2020) 109665.
[75] J. Yao, X. Zeng, Z. Wang, Chem. Eng. J. 330 (2017) 345–354.
[76] Y. Wang, S. Liu, R. Li, et al., J. Environ. Sci. 43 (2016) 54–60.
[77] L. Ge, P. Zhang, C. Halsall, et al., Water Res. 149 (2019) 243–250.
[78] X. Long, Z. Xiong, R. Huang, et al., Appl. Catal. B 317 (2022) 121716.
[79] Z. Xiong, Y. Jiang, Z. Wu, G. Yao, B. Lai, Chem. Eng. J. 421 (2021) 127863.
[80] J. You, C. Zhang, Z. Wu, et al., Chem. Eng. J. 415 (2021) 128890.
[81] Y. Jiang, Z. Xiong, J. Huang, et al., Chin. Chem. Lett. 33 (2021) 415–423.
[82] J. You, W. Sun, S. Su, et al., Chem. Eng. J. 400 (2020) 125915.
[83] L. Zhang, X. Jiang, Z. Zhong, et al., Angew. Chem. Int. Ed. 60 (2021) 21751–21755.
[84] G. Zhang, Y. Xu, C. He, et al., Appl. Catal. B 283 (2021) 119636.
[85] J. Li, X. Liu, C. Liu, et al., J. Taiwan Inst. Chem. Eng. 117 (2020) 93–102.
[86] J. Peng, P. Zhou, H. Zhou, et al., Environ. Sci. Technol. 55 (2021) 9189–9198.
[87] H. Lee, H.I. Kim, S. Weon, et al., Environ. Sci. Technol. 50 (2016) 10134–10142.
[88] H. Wang, W. Guo, B. Liu, et al., Water Res. 160 (2019) 405–414.
[89] B. Liu, W. Guo, H. Wang, et al., Chem. Eng. J. 396 (2020) 125119.
[90] S. Zhu, C. Jin, X. Duan, S. Wang, S.H. Ho, Chem. Eng. J. 393 (2020) 124725.